Effect of low-energy mechanical processing of powder on the formation of structural-phase composition in additive manufacturing of carbon nanotube-reinforced aluminum matrix composites

D. V. Bokaryov, *Post-Graduate Researcher, bokarev.1998@list.ru*
A. S. Raznoschikov, *Post-Graduate Researcher, raznoschikoff.ar@yandex.ru*
A. F. Lelekova, *Junior Researcher, lelekowa.a@yandex.ru*
A. V. Aborkin, *Candidate of Technical Sciences, Associate Professor, aborkin@vlsu.ru*

Vladimir State University named after Alexander and Nikolay Stoletovs (Vladimir, Russia).

In this study, samples were fabricated via selective laser melting (SLM) from composite mixtures based on ASP-30 aluminum powder reinforced with 0.25 vol.% multi-walled carbon nanotubes (CNTs). Powder composites were synthesized through low-energy mechanical processing (LEMP) of the initial constituents in a planetary mill using grinding bodies with diameters of 4 mm and 8 mm. The influence of grinding bodies diameter on particle morphology, structure, and phase composition of the powders was evaluated. It was established that low-energy mechanical processing led to hydrogen and oxygen saturation of the powder mixtures. The mechanism of CNT distribution within the powder mixture during LEMP is described. It has been shown that during SLM of a powder mixture processed with 4 mm diameter milling bodies, the Al_4C_3 phase forms due to the consumption of defective regions of the CNTs, accompanied by an increase in oxygen content and the consequent formation of the Al_2O_3 phase. For the powder mixture processed with 8 mm grinding bodies, a decrease in the structural integrity of CNTs accompanied by reduced oxygen content was observed, indicating significant CNT degradation under laser exposure. Reinforcement of the AlSi10Mg matrix alloy by both exogenous and endogenous phases, along with structural refinement in samples produced from composite powders, resulted in an increase in microhardness by approximately 21–28% compared to the initial powder, along with a 2.2–2.9-fold improvement in wear resistance.

Key words: aluminum matrix composites, carbon nanotubes, selective laser melting, mechanical synthesis, planetary mill, microhardness.

DOI: 10.17580/nfm.2026.01.03

Introduction

Aluminum and its alloys are widely used across various industrial sectors due to their low density, high corrosion resistance, and cost-effectiveness [1]. To enhance the reliability and extend the service life of aluminum-based machine components operating under frictional conditions, their tribological properties – particularly wear resistance – must be improved [2, 3]. One of the effective approaches to improving the wear resistance of aluminum and its alloys is the development of composite materials through reinforcement of the matrix alloy, for instance, with carbon nanotubes (CNTs) [4, 5]. This approach contributes to increased microhardness due to the formation of a refined matrix structure [6]. In addition, CNTs may act as solid lubricants, reducing friction. The development of such composite systems is particularly relevant in the field of additive manufacturing, especially for materials used in selective laser melting (SLM) based on the AlSi10Mg alloy, one of the commercial forms of which is ASP-30 powder. Typically, SLM feedstock powders are characterized by spherical particle morphology and a narrow particle size distribution. The spherical shape ensures uniform powder layer deposition and enhances process stability during SLM fabrication [7].

Industrial production of such powders is commonly achieved via melt atomization. However, fabrication of aluminum- or aluminum alloy-based composite powders reinforced with CNTs using this method is not feasible due to the significant differences in surface tension and density between aluminum and CNTs, as well as their tendency for interfacial reactions. Therefore, such composite powders are typically produced by mechanical processing of the initial components in ball or planetary mills. However, powders obtained through mechanical processing often exhibit irregular particle morphology, which reduces their suitability for SLM. Deviation from spherical particle shape leads to deterioration of technological properties such as flowability and apparent density, potentially preventing the formation of uniform powder layers during SLM. It should be noted that restoring particle sphericity

of such composite powders, for example via plasma spheroidization [8], is impractical due to the formation of in-situ Al_4C_3 phase under elevated temperatures.

Previous studies have investigated SLM of bulk composites based on AlSi10Mg alloy reinforced with CNTs [9–11]. In these works, composite powders were produced by processing initial components in ball [9] and planetary [10, 11] mills. However, the primary focus was placed on optimizing SLM processing parameters, while the influence of mechanical processing on the structure and phase composition of synthesized composite powders has been scarcely addressed. At the same time, the properties of bulk samples are governed not only by SLM parameters but also by powder characteristics such as particle morphology, structural integrity of CNTs, and structural–phase transformations occurring during mechanical processing. Therefore, one of the key practical challenges is to preserve the initial spherical morphology of matrix powder particles during composite preparation. Additionally, it is essential to minimize damage to CNT structural integrity while ensuring sufficient mechanical energy input to achieve homogeneous CNT distribution within the powder mixture [12]. This can be achieved by employing low-energy mechanical processing (LEMP) through controlling the fraction of mechanical energy transferred into the powder mixture being processed, for example, by varying the processing parameters of the initial components and by rationally selecting the diameter of the milling bodies [13]. The set of chosen processing parameters must ensure mixing of the components without significantly affecting the particle shape of the matrix alloy powder and the structural integrity of the CNTs.

The objective of this work is to investigate the effect of grinding bodies diameter on the evolution of morphology and structural–phase composition of composite powders, as well as on the microhardness and wear resistance of bulk composites produced by selective laser melting.

Materials and meth ods

The study employed ASP-30 powder (AlSi10Mg alloy, produced by RUSAL), as well as carbon nanotubes (CNTs), the characterization of which is reported in [14]. LEMP of the initial components was carried out in a Fritsch Pulverisette 6 planetary mill for 1 hour using a steel vial and steel grinding bodies in the form of balls with diameters of 4 mm and 8 mm. Intermediate sampling was performed after 30 minutes of LEMP. The rotational speed of the carrier was 250 rpm. This rotational speed was selected due to the significant reduction in particle sphericity and yield of the usable powder fraction observed at higher rotational speeds [15]. The filling ratio of the milling vial was 0.25 in both cases. The CNT content in the powder mixture was 0.25 vol.% (0.21 wt.%). The initial ASP-30 powder and the synthesized composite powders were sieved through a 63 μm mesh.

The structural and phase composition of the powder composites was analyzed using *X*-ray diffraction (XRD) on a Bruker D8 Advance diffractometer with a Cu Kα radiation source. The morphology of the initial and milled powder particles was examined using a Quanta 200-3D scanning electron microscope. Quantitative evaluation of particle sphericity was performed using the ImageJ software. The sphericity index was defined as the ratio of the average radius of curvature of the particle corners to the radius of the largest inscribed circle within the particle silhouette. The structural integrity of CNTs was evaluated semi-quantitatively based on the intensity ratio of the *D* and *G* bands in Raman spectra obtained using an Ntegra Spectra system with a laser wavelength of 473 nm. The content of aluminum oxide phase in powders and bulk samples was calculated based on oxygen content measurements performed using a METAVAK-AK analyzer. Hydrogen content in powders and bulk samples was measured using a METAVAK-V system.

Bulk specimens for subsequent microstructural analysis, microhardness testing, and wear resistance evaluation were fabricated by selective laser melting (SLM) using a Concept Laser M2 system. The samples were rectangular plates with dimensions of 25 × 3 × 10 mm. The SLM system was equipped with a ytterbium fiber laser operating at a wavelength of 1.07 μm, with a beam spot diameter of 100 μm in the processing zone. Fabrication was carried out in a nitrogen atmosphere, with oxygen content not exceeding 0.7%. The powder layer thickness was 30 μm, and the hatch spacing was 105 μm. The laser power was 190 W, and the scanning speed was 1500 mm/s. No post-processing heat treatment was applied.

The bulk porosity of the samples was determined using the hydrostatic weighing method. Microhardness measurements were performed using a CSM Micro-Combi Tester via instrumented indentation according to the Vickers method. The applied load was 100 mN with a dwell time of 10 s. The results were averaged over 10 measurements.

Wear rate was evaluated under dry sliding conditions using a ball-on-plate configuration, where the SLM specimens were tested against a 6 mm diameter bearing steel (ShKh15) ball on a CSM Instruments tribometer. Tests were conducted in reciprocating mode under a normal load of 10 N and a constant sliding speed of 0.1 m/s. The total sliding distance in all experiments was 100 m. Wear track profiles were recorded using a Mitutoyo Surftest SJ-201 profilometer. The specific wear rate (k_s) was calculated as the ratio of volume loss to the product of applied load and sliding distance.

Results and discussion

SEM micrographs illustrating the particle morphology of the ASP-30 powder and the corresponding composite before and after low-energy mechanical processing (LEMP) with grinding bodies of 4 mm and 8 mm in diameter are presented in **Fig. 1**. The SEM images also include the values of the particle sphericity index.

As shown in **Fig. 1, *a***, the initial ASP-30 powder exhibited a predominantly spherical particle morphology

with a smooth surface. The average particle size was approximately 30 μm. Some particles, however, contained satellites smaller than 5 μm, resulting in a sphericity index slightly below unity. In the composite mixture prior to LEMP **(Fig. 1, *b*)**, CNTs were located on the surface of ASP-30 particles in the form of bundles with a thickness of approximately 5 μm and lengths reaching several hundred micrometers. LEMP had a pronounced effect on both particle shape and size distribution. First, a roughening of the particle surface morphology and the disappearance of satellites were observed **(Fig. 1, *c*)**. Second, the emergence of a fraction of plate-like particles within the powder mixture was detected **(Fig. 1, *d*)**. Increasing the diameter of the grinding bodies led to a decrease in the sphericity index. This can be attributed to the increased mass of individual grinding bodies, which results in higher specific impact energy and, consequently, a greater degree of particle deformation during "ball-vial" and "ball-ball" collisions. It is also important to note that CNTs were not detected in SEM images of the powder mixtures after LEMP.

The results of *X*-ray diffraction (XRD) analysis of the initial ASP-30 powder and composite powders subjected to LEMP with 4 mm and 8 mm grinding bodies are shown in **Fig. 2, *a***. The diffraction patterns exhibited qualitatively similar features, with peaks corresponding to the α-solid solution based on Al, Si, Mg_2Si, and γ-Al_2O_3. No diffraction signal from the reinforcing CNT phase was observed due to its low content. Analysis of the full width at half maximum (FWHM) of the (111) peak of the α-Al solid solution revealed its increase after LEMP. This indicates a reduction in the coherent scattering domain size of the aluminum alloy, which is attributed to severe plastic deformation of the particle surface layer and/or a high degree of deformation of fine particles and satellites.

Typical Raman spectra of the initial ASP-30 powder, composite mixtures after LEMP with 4 mm and 8 mm grinding bodies, and the initial CNTs are shown in **Fig. 2, *b***. The initial ASP-30 powder is characterized by a peak at approximately 520 cm^{-1} corresponding to silicon. The spectra of the initial CNTs exhibit the characteristic *D*, *G*, and 2*D* bands at ~1360 cm^{-1}, ~1570 cm^{-1}, and

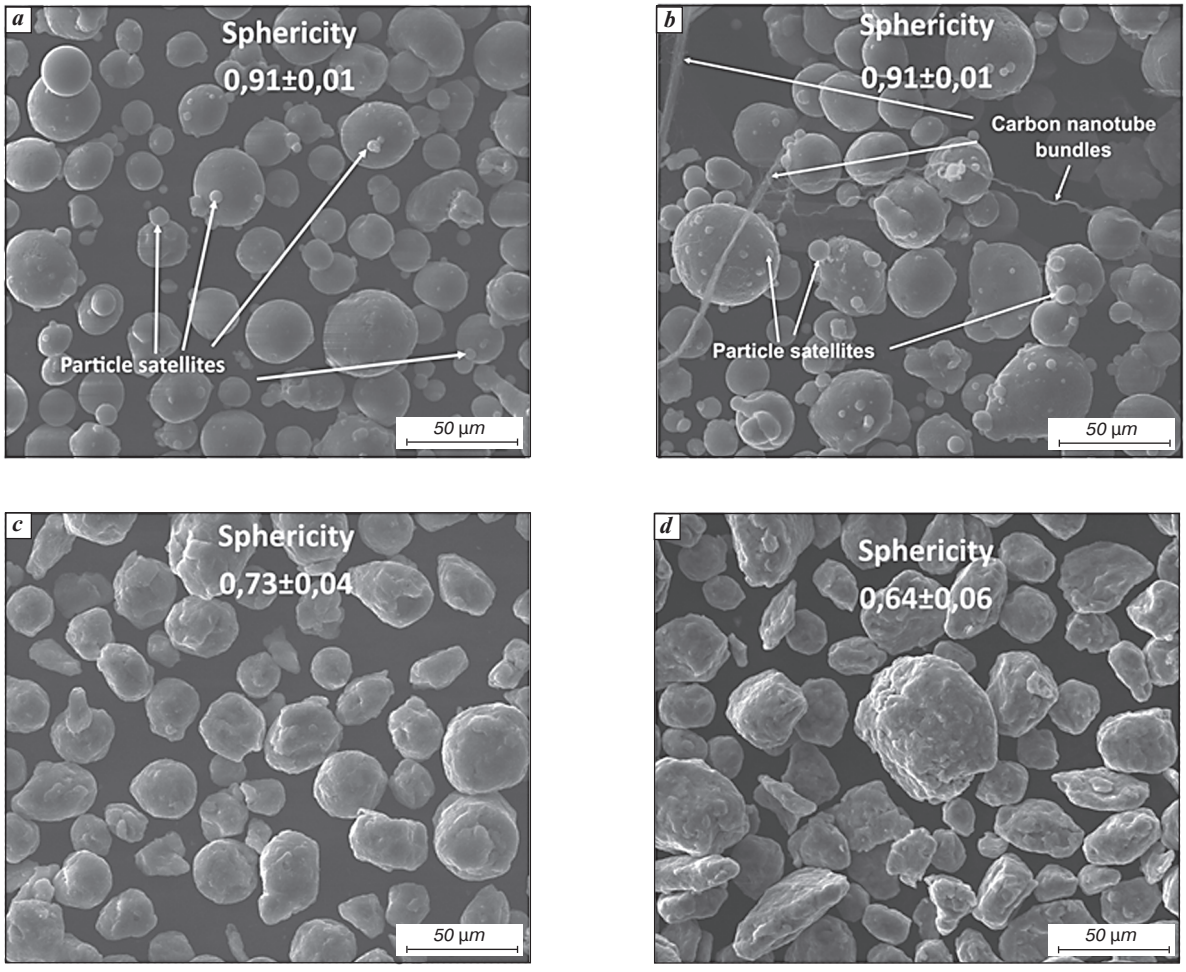

Fig. 1. SEM images of the initial ASP-30 powder (*a*), composite mixture prior to processing (*b*), composite mixture after LEMP with 4 mm balls (c), and composite mixture after mechanical processing with 8 mm balls (*d*)

~2710 cm^{-1}, respectively. Based on the intensity ratio of the *D* and *G* bands ($I_D/I_G = 0.25$), the initial CNTs possess a low defect density. However, LEMP of the powder mixtures resulted in an increase in CNT defectiveness (see **Table**). Specifically, after processing with 4 mm balls, the I_D/I_G ratio increased to 0.65, and to 0.76 after processing with 8 mm balls. In comparison with the spectrum of the initial CNTs, the 2*D* band – typically observed in regions of CNT agglomeration [16] – was absent in the spectra of the composite powders. No peaks corresponding to aluminum carbide were detected in the spectra of the composite powders, indicating the absence of interfacial reactions between the aluminum matrix and CNTs during LEMP. Thus, Raman spectroscopy confirms the presence of CNTs in the composite powder mixtures. Considering the absence of CNTs in SEM images, it can be hypothesized that CNTs are distributed on the surface of powder particles but are covered by a layer of aluminum alloy. This layer likely forms on the surface of larger particles through plastic deformation and welding of satellites and finer particles. SEM data and schematic representations illustrating the proposed mechanism of CNT distribution during LEMP are presented in **Fig. 3**.

Prior to LEMP, the powder exhibited a spherical particle morphology with a significant number of satellites, while CNTs were present between particles in the form of bundles several hundred micrometers in length and several micrometers in thickness. After 30 minutes of LEMP, satellites were no longer observed in SEM images, as they were detached from the host particles. Concurrently, dispersion of CNTs over the particle surfaces occurred. After 60 minutes of LEMP, CNTs were no longer detectable on the particle surfaces. It is likely that during the additional 30 minutes of processing, satellites – transformed into thin flakes – underwent plastic welding with larger powder particles, thereby encapsulating the CNTs beneath them. Further increase in processing time to 90 minutes did not improve the distribution of the reinforcing phase, as the position of CNTs had already become fixed. Therefore, the LEMP duration in the present study was limited to 1 hour.

Analysis of oxygen and hydrogen content in powders after low-energy mechanical processing (LEMP) revealed

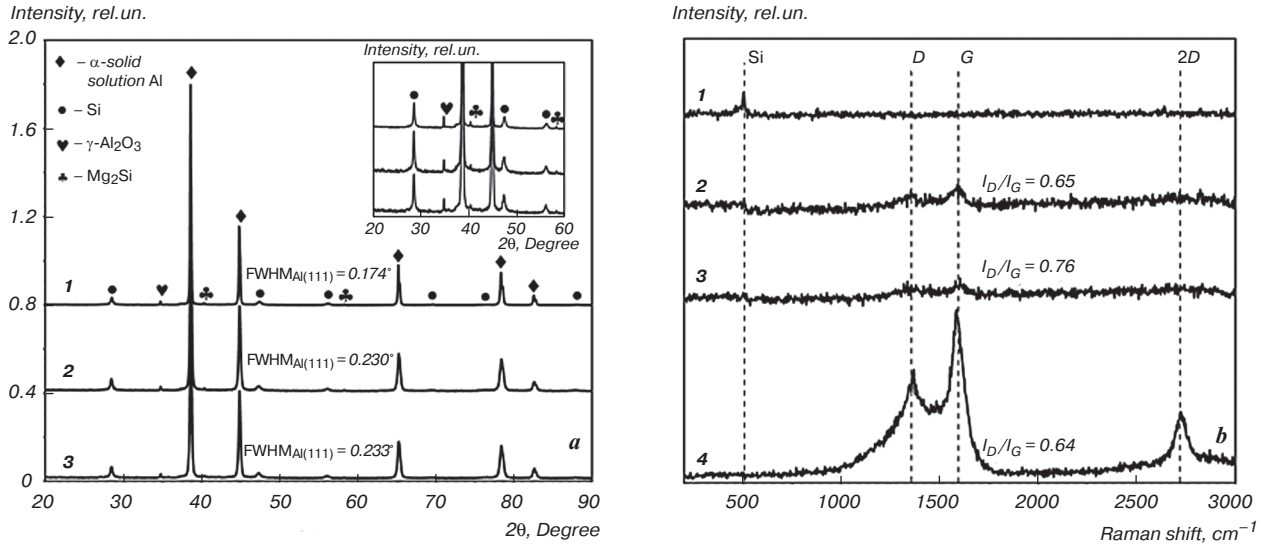

Fig. 2. Results of *X*-ray diffraction analysis (*a*) and Raman spectroscopy (*b*) of powder materials. Designations: *1* – initial ASP-30; *2* – composite mixture after LEMP with 4 mm balls; *3* – composite mixture after LEMP with 8 mm balls; *4* – initial CNTs

Table
Characteristics of powders and SLM-fabricated samples

	O, wt.%	Al_2O_3, vol.%	*H*, wt.%	I_D/I_G	Porosity, %	$HV_{0.1}$	k_S, $mm^3 \cdot N^{-1} \cdot m^{-1}$
Powder							
ASP-30	0.076	0.12	0.007	–	–	–	–
LEMP ∅4 mm	0.286	0.51	0.016	0.65 ±0.1	–	–	–
LEMP ∅8 mm	0.398	0.78	0.014	0.76±0.2	–	–	–
SLM sample							
ASP-30	0.080	0.12	0.012	–	0.7±0.1	130 ±19	$3.84 \cdot 10^{-3}$
LEMP ∅4 mm	0.323	0.60	0.037	0.52±0.14	8.5±0.1	182±28	$1.34 \cdot 10^{-3}$
LEMP ∅8 mm	0.221	0.38	0.017	0.94±0.21	8.1±0.1	165±13	$1.72 \cdot 10^{-3}$

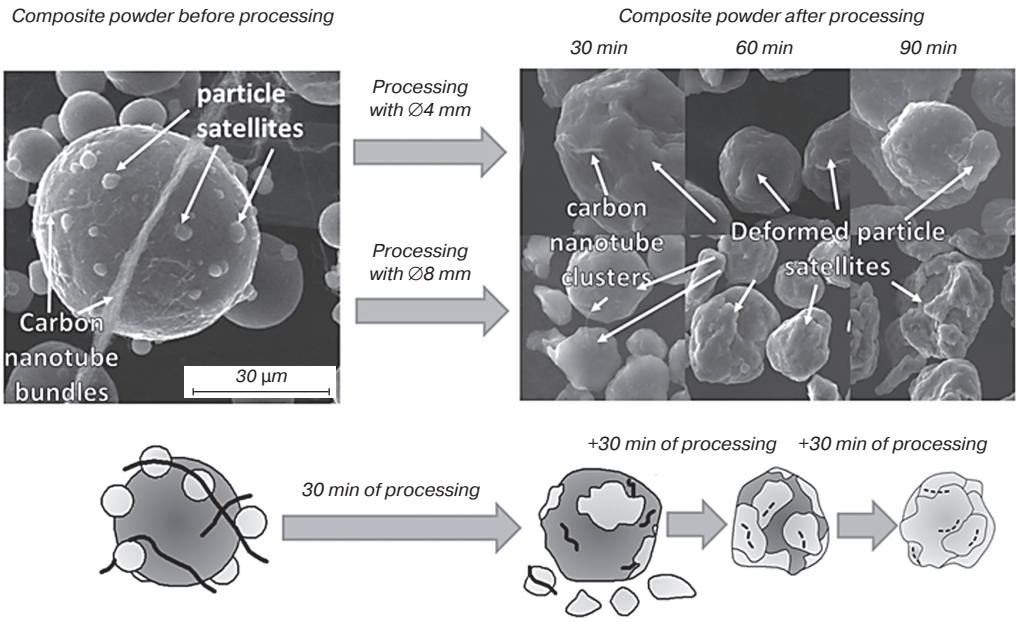

Fig. 3. Schematic representation of the CNT distribution mechanism during LEMP

a significant increase compared to the initial ASP-30 powder (see **Table**). Specifically, after LEMP, the oxygen content increased by approximately 3.8–5.2 times, while the hydrogen content increased by approximately 2.0–2.3 times. Moreover, an increase in the energy intensity of LEMP, achieved by increasing the diameter of the grinding bodies, resulted in a further rise in oxygen and hydrogen content in the processed powder mixtures. Nevertheless, despite the substantial increase in oxygen content after LEMP, its value did not exceed 0.4 wt.%. Given the low solubility of oxygen in aluminum, it can be reasonably assumed that oxygen is predominantly present in the form of Al_2O_3. Under this assumption, the volume fraction of this phase after LEMP with different grinding bodies diameters increases to approximately 0.51–0.78 vol.%. It is important to note that an increased content of in-situ Al_2O_3 in the powder mixture may have a beneficial effect on the mechanical properties of the resulting material. In contrast, the increase in hydrogen content (see **Table**) should be considered a detrimental factor, as it is likely to promote porosity formation in bulk samples and negatively affect their mechanical performance.

Microstructural analysis of SLM-fabricated samples revealed a characteristic cellular structure formed by semicircular melt pools. Refinement of the microstructure was observed at the boundaries of these cells. In all analyzed SLM samples, irregularly shaped pores were detected, which formed due to shrinkage of the interdendritic liquid during solidification. Additionally, spherical pores were observed, originating from the solidification of gas bubbles within the overheated melt pool. The volumetric porosity of the SLM sample fabricated from the initial ASP-30 powder was 0.7 ± 0.1%, whereas the composite SLM samples exhibited porosity values approximately one order of magnitude higher (see **Table**). The maximum porosity of 8.5% was observed in samples produced from composite powder processed with 4 mm grinding bodies. The increase in porosity of SLM samples can be attributed to the elevated hydrogen content in composite powders after LEMP. It should be noted that a decrease in the sphericity of powder particles can affect its apparent density and the uniformity of the powder layer deposition during SLM. However, during SLM printing, no differences in the uniformity of deposition of powder mixtures with different particle sphericity values were visually observed. Moreover, the SLM-fabricated specimens exhibited similar porosity levels. It can therefore be stated that, in this case, there are no limitations regarding the practical applicability of the obtained powders with reduced sphericity for the fabrication of components by the SLM method.

X-ray diffraction analysis of the SLM samples revealed several notable features (see **Fig. 4, *a***). First, the appearance of additional diffraction peaks corresponding to Si was observed (see inset in **Fig. 4, *a***). This is likely associated with rapid crystallization processes from the overheated matrix alloy during SLM, leading to phase transformations and changes in the crystal structure of silicon [17]. Second, a redistribution of diffraction peak intensities was observed in the SLM sample produced from the initial ASP-30 powder. For example, the intensity ratio of the (111) and (200) reflections of aluminum changed, indicating the formation of a preferred crystallographic texture. Considering the absence of such changes in SLM samples produced from composite powders, it can be inferred that CNTs influence the structural evolution of the AlSi10Mg alloy during solidification.

Furthermore, broadening of the (111) diffraction peak in the patterns of composite samples **(Fig. 4, *a*)** indirectly indicates grain boundary pinning during crystallization, which may also be associated with the presence of CNTs.

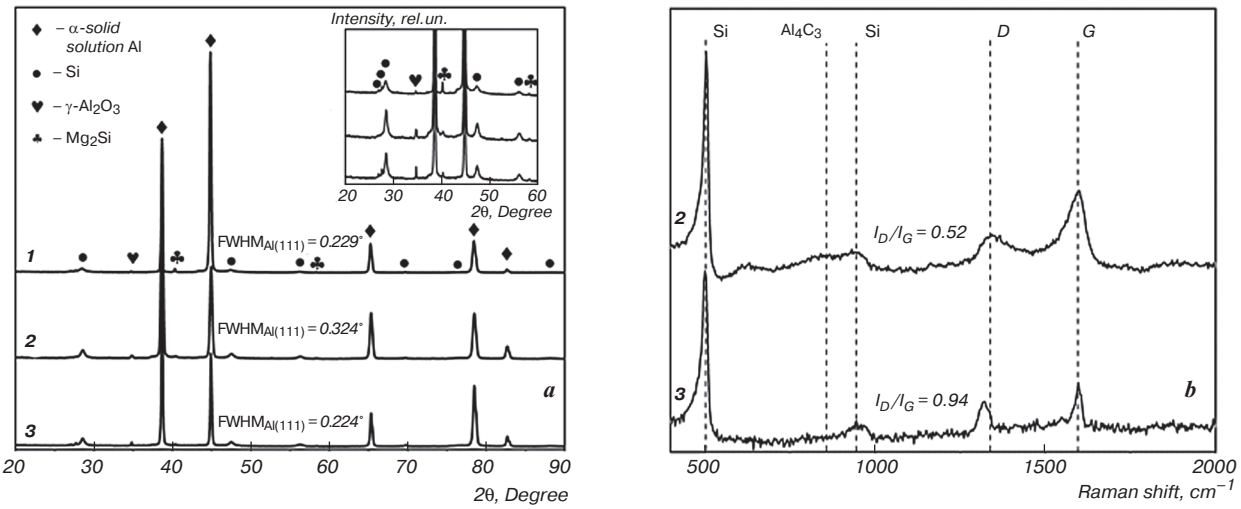

Fig. 4. Results of *X*-ray diffraction analysis (*a*) and Raman spectroscopy (*b*) of SLM-fabricated samples. Designations: *1* – initial ASP-30; *2* – composite mixture after LEMP with 4 mm grinding bodies; *3* – composite mixture after LEMP with 8 mm grinding bodies

Raman spectra of SLM samples fabricated from composite powders exhibited additional bands at approximately 505 cm^{-1} and 945 cm^{-1} (see **Fig. 4, *b***). Similar bands were reported in [18], where they were attributed to endogenous oxide phases of silicon and aluminum. However, taking into account the findings of [19] regarding the influence of residual stresses on peak shifts and broadening in Raman spectra of hypereutectic Al – Si alloys quenched from above the liquidus temperature, we suggest that these bands should instead be attributed to silicon.

Simultaneously, Raman spectra exhibited signals corresponding to the *D* and *G* bands of the exogenous reinforcing phase – CNTs **(Fig. 4, b)**. Notably, after LEMP with 4 mm grinding bodies, the intensities of the *D* and *G* bands were higher than those observed after processing with 8 mm bodies. The I_D/I_G ratio in SLM samples also changed compared to the corresponding powder composite mixtures. For instance, in SLM samples produced from powders processed with 4 mm grinding bodies, the I_D/I_G ratio decreased to 0.52. This behavior can be attributed to the fact that structural defects in CNTs serve as carbon sources and preferential sites for the formation of exogenous carbide phases, particularly Al_4C_3 [20, 21]. This is further supported by the formation of a plateau in the vicinity of ~860 cm^{-1} in the Raman spectrum **(Fig. 4, *b*)**. In contrast, for SLM samples obtained from powders processed with 8 mm grinding bodies, the I_D/I_G ratio increased to 0.94. This indicates that, during SLM, CNT degradation processes occur; however, no simultaneous formation of in-situ Al_4C_3 phase was detected in the spectra.

The results of oxygen and hydrogen content analysis in SLM samples are presented in Table 1. It can be observed that the fraction of aluminum oxide in the SLM sample produced from the initial ASP-30 powder remained unchanged after consolidation, whereas the hydrogen content nearly doubled. After consolidation of composite powder processed with 4 mm grinding bodies, the fraction of aluminum oxide increased to 0.6 vol.%, while the hydrogen content increased by approximately 2.3 times. In contrast, for samples produced from powder processed with 8 mm grinding bodies, the hydrogen content increased by approximately 1.5 times, while the aluminum oxide fraction decreased by approximately twofold compared to the powder state. The latter effect may be attributed to partial разрушение or evaporation of the oxide film, potentially involving carbon from structurally degraded CNTs. According to [22], the temperature in the melt pool under laser irradiation can reach approximately 1758 °C.

Structural and phase transformations occurring in powders during LEMP and subsequent SLM significantly influenced the microhardness of the composite samples. Specifically, the microhardness increased by 28% and 21% for samples processed with 4 mm and 8 mm grinding bodies, respectively, compared to the sample fabricated from the initial ASP-30 powder. For proper comparison with results reported by other research groups, the volumetric reinforcement efficiency parameter (*R*) was employed, calculated according to the methodology described in [23] (see **Table**). Previous studies [24–26] reported microhardness increases exceeding 25% for SLM-fabricated samples reinforced with 1 wt.% CNTs, 0.5 wt.% carbon fiber, or 0.5 wt.% graphene, respectively, with corresponding reinforcement efficiencies (*R*) of 26%, 46%, and 92%. The SLM samples obtained in the present study demonstrated higher reinforcement efficiency despite a lower volume fraction of the reinforcing phase. Specifically, for samples produced from powders processed with 4 mm grinding bodies, $R = 161\%$, whereas for 8 mm bodies, $R = 110\%$. The increase in microhardness can be attributed to a combined strengthening mechanism involving exogenous

reinforcement by CNTs, in-situ formation of ceramic phases Al_2O_3 and Al_4C_3, and grain refinement of the matrix alloy due to grain boundary pinning during solidification. The increased hardness of composite SLM samples also contributed to enhanced wear resistance. As shown in **Table**, the specific wear rate decreased by approximately 2.9 and 2.2 times for SLM samples produced from composite powders processed with 4 mm and 8 mm grinding bodies, respectively, compared to the sample fabricated from the initial ASP-30 powder.

A comprehensive analysis indicates that, under the conditions considered in this study, the use of smaller-diameter grinding bodies is preferable. It should be noted that the selection of an optimal grinding bodies diameter, as one of the key factors determining the energy intensity of mechanical processing, constitutes a subject for further dedicated investigation.

Conclusions

1. The effect of grinding bodies diameter during low-energy mechanical processing (LEMP) with 4 mm and 8 mm balls on the evolution of morphology and structural–phase composition of composite powders based on the AlSi10Mg alloy reinforced with 0.25 vol.% CNTs was investigated. It was shown that increasing the grinding bodies diameter from 4 to 8 mm leads to a decrease in particle sphericity from 0.73 to 0.61, compared to 0.91 for the initial powder. LEMP was found to result in hydrogen and oxygen saturation of the powder mixtures. Relative to the initial powder, the oxygen content increased by approximately 3.8–5.2 times, while the hydrogen content increased by approximately 2.0–2.3 times for processing with 4 mm and 8 mm grinding bodies, respectively. In addition, the influence of grinding bodies size on the defectiveness of the exogenous reinforcing phase was evaluated. The I_D/I_G ratio increased from 0.25 (initial CNTs) to 0.65 and 0.76 after processing with 4 mm and 8 mm grinding bodies, respectively. A mechanism describing CNT distribution within the powder mixture during LEMP was proposed.

2. Bulk samples were fabricated by selective laser melting (SLM), exhibiting a characteristic cellular microstructure formed by semicircular melt pools. Microstructural refinement was observed at the boundaries of the cellular structure. The presence of the exogenous reinforcing phase influenced the solidification behavior of the AlSi10Mg alloy and contributed to microstructural refinement. It has been established that during selective laser melting of the powder mixture processed with 4 mm diameter milling bodies, the formation of an in-situ Al_4C_3 phase occurs through the consumption of defective regions of the exogenous phase. Additionally, an increase in oxygen content was observed, leading to the formation of the in-situ Al_2O_3 phase up to 0.6 vol.%. For the powder mixture processed with 8 mm grinding bodies, a decrease in the structural integrity of the exogenous phase accompanied by a reduction in oxygen content was observed, indicating degradation of the reinforcing phase under laser irradiation.

3. The combined reinforcement of the AlSi10Mg matrix alloy by exogenous and endogenous phases, together with microstructural refinement in samples produced from composite powders, resulted in an increase in microhardness by approximately 21–28% compared to the sample fabricated from the initial powder. The highest hardness values were observed in samples produced from composite mixtures subjected to LEMP with smaller-diameter grinding bodies. An improvement in wear resistance by approximately 2.9 and 2.2 times was established for composite samples obtained from powders processed with 4 mm and 8 mm grinding bodies, respectively.

Acknowledgements

The research was carried out within the state assignment in the field of scientific activity of the Ministry of Science and Higher Education of the Russian Federation (theme FZUN-2024-0004, state assignment of the VISU).

References

1. Ostojic S., Traverso M. From Aluminium to Composites: a Comparative Social Life Cycle Assessment of Automotive Lightweight Components. *Journal of Cleaner Production*. 2025. Vol. 523. 146361.

2. Divakar S., Sardar S., Sah S., Das D. A. State-Of-The-Art Review on SiC and MWCNTs Reinforced Hybrid Metal Matrix Composites: Processing, Properties, and Applications. *Hybrid Advances*. 2025. Vol. 10. 100454.

3. Aranke O., Gandhi C., Dixit N., Kuppan P. Influence of Multiwall Carbon Nanotubes (MWCNT) on Wear and Coefficient of Friction of Aluminium (Al 7075) Metal Matrix Composite. *Materials Today: Proceedings*. 2018. Vol. 5, Iss. 2, Pt. 2. P. 7748–7757.

4. Romanov A. D., Romanova E. A., Mironov A. A., Kikeev V. A., Obiedkov A. M., Kaverin B. S., Vilkov I. V. Developing a Technology for Obtaining an Aluminum Matrix Composite Reinforced with Multi-Walled Carbon Nanotubes. *Metallurgist*. 2024. Vol. 68. Iss. 3. pp. 427–432.

5. Romanov A. D., Romanova E. A., Vilkov I. V., Obedkov A. M., Semenov N. M., Kaverin B. S., Kovylin R. S. Technology for Producing Aluminum-Matrix Composite Material Reinforced with Multi-Wall Carbon Nanotubes. *Metallurgist*. 2022. Vol. 66. Iss. 5-6. pp. 681–687.

6. Kremlev K. V., Ob"edkov A. M., Semenov N. M., Kaverin B. S., Ketkov S. Yu., Gusev S. A., Yunin P. A., Elkin A. I., Aborkin A. V. The Gas-Phase Synthesis of a New Functional Hybrid Material on the Basis of Multiwalled Carbon Nanotubes Decorated with Faceted Aluminum Nanocrystals. *Technical Physics Letters*. 2018. Vol. 44. pp. 865–868.

7. Jeon T. J., Hwang T. W., Yun H. J., VanTyne C. J., Moon Y. H. Control of Porosity in Parts Produced by a Direct Laser Melting Process. *Applied Sciences*. 2018. Vol. 8, Iss. 12. 2573.

8. Higashi M., Ozaki T. Selective Laser Melting of MoSiBTiC Alloy with Plasma-Spheroidized Powder: Microstructure and

Mechanical Property. *Materials Characterization*. 2021. Vol. 172. 110888.

9. Wang, L., Chen, T., Wang, S. Microstructural Characteristics and Mechanical Properties of Carbon Nanotube Reinforced AlSi10Mg Composites Fabricated by Selective Laser Melting. *Optik*. 2017. Vol. 143. 173–179.

10. Gu D., Rao X., Dai D., Ma C., Xi L., Lin K. Laser Additive Manufacturing of Carbon Nanotubes (CNTs) Reinforced Aluminum Matrix Nanocomposites: Processing Optimization, Microstructure Evolution And Mechanical Properties. *Additive Manufacturing*. 2019. Vol. 29. pp. 2–10.

11. Aboulkhair N. T., Simonelli M., Salama E., Rance G. A., Neate N. C., Tuck C. J., Esawi A. M. K., Hague R. J. M. Evolution of Carbon Nanotubes and Their Metallurgical Reactions in Al-based Composites in Response to Laser Irradiation During Selective Laser Melting. *Materials Science and Engineering: A*. 2019. Vol. 765. 138307.

12. Aborkin A. V., Khor'kov K. S., Ob"edkov A. M., Kremlev K. V., Izobello A. Yu., Volochko A. T., Alymov M. I. Evolution of Multiwalled Carbon Nanotubes and Related Nanostructures during the Formation of Alumomatrix Composite Materials. *Technical Physics Letters*. 2019. Vol. 45. pp. 20–23.

13. Gusev V. G., Sobol'kov A. V., Aborkin A. V., Alymov M. I. Simulation of the Energy–Force Parameters of Planetary Ball Mill Processing and Estimation of Their Influence on the Particle Size in an AMg2 Alloy/Graphite Composite Powder. *Russian Metallurgy (Metally)*. 2019. Vol. 2019. pp. 24–30.

14. Ob'edkov A. M., Kaverin B. S., Egorov V. A., Semenov N. M., Ketkov S. Yu., Domrachev G. A., Kremlev K. V., Gusev S. A., Perevezentsev V. N., Moskvichev A. N., Moskvichev A. A., Rodionov A. S. Macro-Cylinders Based on Radially Oriented Multi-Walled Carbon Nanotubes. *Letters on Materials*. 2012. Vol. 2. pp. 152–156.

15. Bokarev D. V., Aborkin A. V. Influence of the Energy Intensity of Processing in a Planetary Ball Mill on the Structure of ASP-30 Powder. *Progressive Foundry Technologies: Proceedings of the XII International Scientific and Practical Conference*. Moscow: National University of Science and Technology MISIS, 2024, pp. 443–449.

16. Wu J., Lin M. L., Cong X., Liu H. N., Tan P. H. Raman Spectroscopy of Graphene-Based Materials and Its Applications in Related Devices. *Chemical Society Reviews*. 2018. Vol. 47, Iss. 5. pp. 1822–1873.

17. Wang W., Bian X., Qin J., Syliusarenko S. I. The Atomic-Structure Changes in Al-16 pct Si Alloy Above the Liquidus. *Metallurgical and Materials Transactions A*. 2000. Vol. 31.pp. 2163–2168.

18. Shinkaryov A. S., Ozherelkov D. Y., Pelevin I. A., Eremin S. A., Anikin V. N., Burmistrov M. A., Chernyshikhin S. V., Gromov A. A., Nalivaiko A. Y. Laser Fusion of Aluminum Powder Coated with Diamond Particles via Selective Laser Melting: Powder Preparation and Synthesis Description. *Coatings*. 2021. Vol. 11, Iss. 10. 1219.

19. Robles Hernandez F., Sokolowski J., Cruz Rivera J. de J. Micro-Raman Analysis of the Si Particles Present in Al-Si Hypereutectic Alloys in Liquid and Semi-Solid States. *Advanced Engineering Materials*. 2007. Vol. 9. pp. 46–51.

20. Li Z., Li B.-Q., Bai P., Liu B., Wang Y. Research on the Thermal Behaviour of a Selectively Laser Melted Aluminium Alloy: Simulation and Experiment. *Materials*. 2018. Vol. 11. 1172.

21. Aborkin A., Babin D., Bokaryov D. Control of Al_4C_3 Phase Formation in Aluminum Matrix Composites Reinforced with Carbon Nanostructures. *E3S Web of Conferences*. 2023. Vol. 431. 06012.

22. Chen B., Shen J., Ye X., Imai H., Umeda J., Takahashi M., Kondoh K. Solid-State Interfacial Reaction and Load Transfer Efficiency in Carbon Nanotubes (CNTs)-Reinforced Aluminum Matrix Composites. *Carbon*. 2017. Vol. 114. P. 198–208.

23. Chen B., Jia L., Li S., Imai H., Takahashi M. Kondoh K. In Situ Synthesized Al_4C_3 Nanorods with Excellent Strengthening Effect in Aluminum Matrix Composites. *Advanced Engineering Materials*. 2014. Vol. 16. pp. 972–975.

24. Luo S., Li R., He P., Yue H., Gu J. Investigation on the Microstructure and Mechanical Properties of CNTs-AlSi10Mg Composites Fabricated by Selective Laser Melting. *Materials*. 2021. Vol. 14. Iss. 4. pp. 1–15.

25. Ozherelkov D. Y., Pelevin I. A., Nalivaiko A. Y., Zotov B. O., Fedorenko L. V., Gromov A. A. Use of Carbon Nanofibers in the Additive Manufacturing of Aluminum Matrix Composites. *Russian Metallurgy (Metally)*. 2023. Vol. 10. pp. 1374–1381.

26. Yu T., Liu J., He Y., Tian J., Chen M., Wang Y. Microstructure and Wear Characterization of Carbon Nanotubes (CNTs) Reinforced Aluminum Matrix Nanocomposites Manufactured Using Selective Laser Melting. *Wear*. 2021. Vol. 476. 203581.